Methamphetamine Enhances *Cryptococcus neoformans* Pulmonary Infection and Dissemination to the Brain

Dhavan Patel,[a] Gunjan M. Desai,[a] Susana Frases,[b] Radames J. B. Cordero,[c,d] Carlos M. DeLeon-Rodriguez,[e] Eliseo A. Eugenin,[f,g] Joshua D. Nosanchuk,[e,h] Luis R. Martinez[a,e,h]

Department of Biomedical Sciences, Long Island University Post, Brookville, New York, USA[a]; Laboratório de Ultraestrutura Celular Hertha Meyer, Instituto de Biofísica Carlos Chagas Filho,[b] Instituto de Bioquímica Médica,[c] and Instituto de Microbiologia,[d] Universidade Federal do Rio de Janeiro, Rio de Janeiro, Brazil; Public Health Research Institute (PHRI)[f] and Department of Microbiology and Molecular Genetics,[g] UMDNJ, Newark, New Jersey, USA; Department of Microbiology and Immunology[e] and Division of Infectious Diseases, Department of Medicine,[h] Albert Einstein College of Medicine, Bronx, New York, USA

ABSTRACT Methamphetamine (METH) is a major addictive drug of abuse in the United States and worldwide, and its use is linked to HIV acquisition. The encapsulated fungus *Cryptococcus neoformans* is the most common cause of fungal meningitis in patients with AIDS. In addition to functioning as a central nervous system stimulant, METH has diverse effects on host immunity. Using a systemic mouse model of infection and *in vitro* assays in order to critically assess the impact of METH on *C. neoformans* pathogenesis, we demonstrate that METH stimulates fungal adhesion, glucuronoxylomannan (GXM) release, and biofilm formation in the lungs. Interestingly, structural analysis of the capsular polysaccharide of METH-exposed cryptococci revealed that METH alters the carbohydrate composition of this virulence factor, an event of adaptation to external stimuli that can be advantageous to the fungus during pathogenesis. Additionally, we show that METH promotes *C. neoformans* dissemination from the respiratory tract into the brain parenchyma. Our findings provide novel evidence of the impact of METH abuse on host homeostasis and increased permissiveness to opportunistic microorganisms.

IMPORTANCE Methamphetamine (METH) is a major health threat to our society, as it adversely changes people's behavior, as well as increases the risk for the acquisition of diverse infectious diseases, particularly those that enter through the respiratory tract or skin. This report investigates the effects of METH use on pulmonary infection by the AIDS-related fungus *Cryptococcus neoformans*. This drug of abuse stimulates colonization and biofilm formation in the lungs, followed by dissemination of the fungus to the central nervous system. Notably, *C. neoformans* modifies its capsular polysaccharide after METH exposure, highlighting the fungus's ability to adapt to environmental stimuli, a possible explanation for its pathogenesis. The findings may translate into new knowledge and development of therapeutic and public health strategies to deal with the devastating complications of METH abuse.

Methamphetamine (METH) is an extremely addictive stimulant of the central nervous system (CNS). METH abuse is a significant public health problem in the United States. It is estimated that >12.3 million Americans (4.9% of persons aged 12 or older) have used METH at least once, 1.4 million aged 12 or older (0.6% of the U.S. population) used METH during the past year, and 600,000 (0.2% of the U.S. population) used it during the past month (1). METH abuse may also facilitate the progression of HIV infection, as HIV-infected METH users have more pronounced neuronal injury and cognitive impairment than HIV-infected individuals who do not use the drug (2, 3). The transmission of HIV (4, 5), hepatitis B and C (6), and other transmissible diseases is a possible serious infectious consequence of METH use. METH adversely impacts immunological responses, which might contribute to the higher rate and more rapid progression of certain infections in drug abusers. We recently demonstrated that METH administration modifies leukocyte proliferation and cytokine production in diverse murine tissues (7). Also, the highest uptake of the drug occurs in lung, and levels are intermediate in brain (8). METH use has profound implications on tissue homeostasis and the capacity of the host to respond to diverse insults, including invading pathogens (7, 8).

The encapsulated AIDS-associated pathogenic fungus *Cryptococcus neoformans* is an excellent model organism for the study of CNS susceptibility to infection due to the availability of tools such as specific antibodies and well-established animal systems. *C. neoformans* enters the host through the respiratory tract. Disease is normally contained by host effector responses, but the fungus is nevertheless responsible for ~1 million cases annually of meningoencephalitis (9), primarily in HIV-infected individuals. *C. neoformans* infection presents formidable problems for the host immune response, including the presence of titan cells in tissue (10), a lack of antibody responsiveness to capsular polysaccharide, and extensive accumulation of polysaccharide in tissue (11). The pres-

ence of glucuronoxylomannan (GXM), the major capsular poly-saccharide of *C. neoformans*, in tissue is believed to be a major contributor to *C. neoformans* pathogenesis since this compound is copiously released during infection and has been associated with a variety of immunosuppressive effects (12). Furthermore, GXM release is essential for cryptococcal biofilm formation (13), a strategy associated with chronic infections as a result of acquired resistance to host immune mechanisms (14) and antimicrobial therapy (15). Biofilm formation by *C. neoformans* follows a discrete sequence of events, including fungal surface adhesion, microcolony formation, and matrix production (13).

During cryptococcosis, fungemia is detected in ~50% of HIV-infected patients (16). The correlation between fungemia and dissemination, including brain invasion, has been made for experimental models of cryptococcosis (17), and fungemia is identified as an independent parameter of failure of host effector responses (16). Brain invasion by *C. neoformans* requires viable yeast cells, and there is evidence of a transcellular passage of the fungus across the blood-brain barrier (BBB) (18, 19). In fact, we recently showed that BBB disruption accelerates transmigration of *C. neoformans* into the brain parenchyma after systemic infection (20). In the present study, we hypothesized that METH in lung tissues exacerbates cryptococcal infection, promoting fungal biofilm formation and dissemination to the CNS. Using a systemic mouse model of infection, we demonstrate that METH stimulates *C. neoformans* adhesion, GXM release, and biofilm formation in the lungs and accelerates fungal cell migration to the brain.

RESULTS

METH exacerbates pulmonary cryptococcosis. Administration of METH significantly accelerated the time to death of *C. neoformans*-infected mice relative to that of control mice ($P < 0.01$). On day 9 postinfection, 100% of METH-treated mice were dead, compared to 50% of the control mice. On average, METH-treated mice died 6 days postinfection versus 9 days postinfection for the control mice (Fig. 1A). In mice infected with 10^6 *C. neoformans* cells, pulmonary fungal burdens in METH-treated animals were significantly higher than in control mice ($P < 0.05$) (Fig. 1B). In addition, GXM was more extensively released by *C. neoformans* in the lungs of METH-treated mice than in those of controls (Fig. 1C).

Histological examination revealed that mice treated with METH prior to infection with 10^6 *C. neoformans* cells had a baseline abnormal morphology characterized by peribronchial inflammation and inflammatory cells present within alveoli (Fig. 1E). This finding suggests that METH deregulates host homeostasis. Significantly, infected METH-treated mice had large numbers of fungal cells and reduced inflammation as well as massive accumulations of fungal polysaccharide. In contrast, the lungs of control mice showed localized inflammation and dense cellular infiltration (Fig. 1D). In summary, our findings demonstrate that METH administration enhances disease progression by increasing pulmonary fungal burden and amassing of polysaccharide, leading to the inhibition of the host cellular infiltrates.

METH enhances fungal adhesion to human epithelial lung cells. We investigated the ability of *C. neoformans* to adhere to A549 epithelial lung cells after METH treatment (Fig. 2). METH significantly increased the ability of cryptococcal cells to adhere to A549 epithelial cells relative to that of untreated cells ($P < 0.05$ and $P < 0.001$ for 25 and 50 μM METH, respectively) (Fig. 2A).

Fluorescence microscopy confirmed that METH enhances the interaction of *C. neoformans* (blue) with epithelial cells (red) compared to the interaction of untreated controls (Fig. 2B), revealing that multiple yeast cells frequently engaged single METH-exposed epithelial cells.

The surface charge of cryptococcal cells was measured (Fig. 2C). Previous studies have shown that the polysaccharide capsule of *C. neoformans* is responsible for a high negative charge on the surfaces of the cells (21). Exposure to increasing concentrations of METH significantly increased the net negative surface charge of the cryptococcal cells (-44.66 ± 6.42 and -49.58 ± 5.87 for 25 and 50 μM METH, respectively) compared to that of nonexposed cryptococcal cells (-29.65 ± 5.74) ($P < 0.05$ and $P < 0.001$ for 25 and 50 μM METH, respectively).

METH enhances GXM release *in vitro*. *C. neoformans* sheds large amounts of polysaccharide into culture media and infected tissues (22). The capsule size of *C. neoformans* H99 cells was measured in cells grown in the presence or absence of METH to determine whether or not this drug altered capsule growth and to assess its effect on the quantity of GXM released in culture. After 24 h, the capsule size of *C. neoformans* cells grown in the presence of METH (2.57 ± 0.52 μm and 2.20 ± 0.66 μm with 25 and 50 μM METH, respectively) was significantly reduced compared with the capsule size of the untreated controls (2.97 ± 0.70 μm) ($P < 0.05$) (Fig. 3A). Conversely, *C. neoformans* polysaccharide capsule release in the presence of METH was significantly greater than in the absence of the drug ($P < 0.05$ and $P < 0.001$ for 25 and 50 μM, respectively) (Fig. 3B). Using light microscopy, we demonstrated that METH significantly reduced the quantity of capsular polysaccharide (Fig. 3C), suggesting that METH stimulates GXM release into the medium.

METH alters *C. neoformans* capsular polysaccharide size and composition. We analyzed the size distribution of polysaccharide from *C. neoformans* capsule molecules cultivated with or without METH (Fig. 4). The capsular polysaccharide molecules of METH-treated yeast cells exhibited, on average, a smaller diameter (941.0 ± 11.9 nm) (Fig. 4B) than those of untreated cells ($1,203.8 \pm 33.2$ nm) (Fig. 4A). Treatment with METH yielded two homogeneous populations of reduced capsular polysaccharide. The size distribution range for each population was 181.1 to 273.9 and 1,590.5 to 2,405.8 nm, with the highest values at 222.7 and 1,956.1 nm, respectively (Fig. 4B). Similarly, two different populations with respect to polysaccharide size were present in untreated cells (Fig. 4A). The size range for each population was 2.03 to 288.1 and 1,405.9 to 3,786.7 nm, with the highest values at 193.8 and 2,089.7 nm, respectively. Using immunofluorescence, we demonstrated a significant reduction in capsule-specific monoclonal antibody (MAb) 18B7 binding to cryptococcal cells treated with METH relative to that of control yeast cells (Fig. 4C), suggesting that METH might be capable of altering capsular polysaccharide synthesis and/or structure, resulting in a different capsular surface with altered epitope density and/or accessibility. METH-induced alterations of the cryptococcal cell surface might have adverse implications on host-pathogen interactions and enhance pathogenesis.

Preparations of cryptococcal polysaccharide capsule material released in culture medium from strain H99 after incubation in the absence or presence of 25 μM METH were analyzed for carbohydrate composition by combined gas chromatography-mass spectrometry (Table 1). METH-treated cultures (514.5 mg/
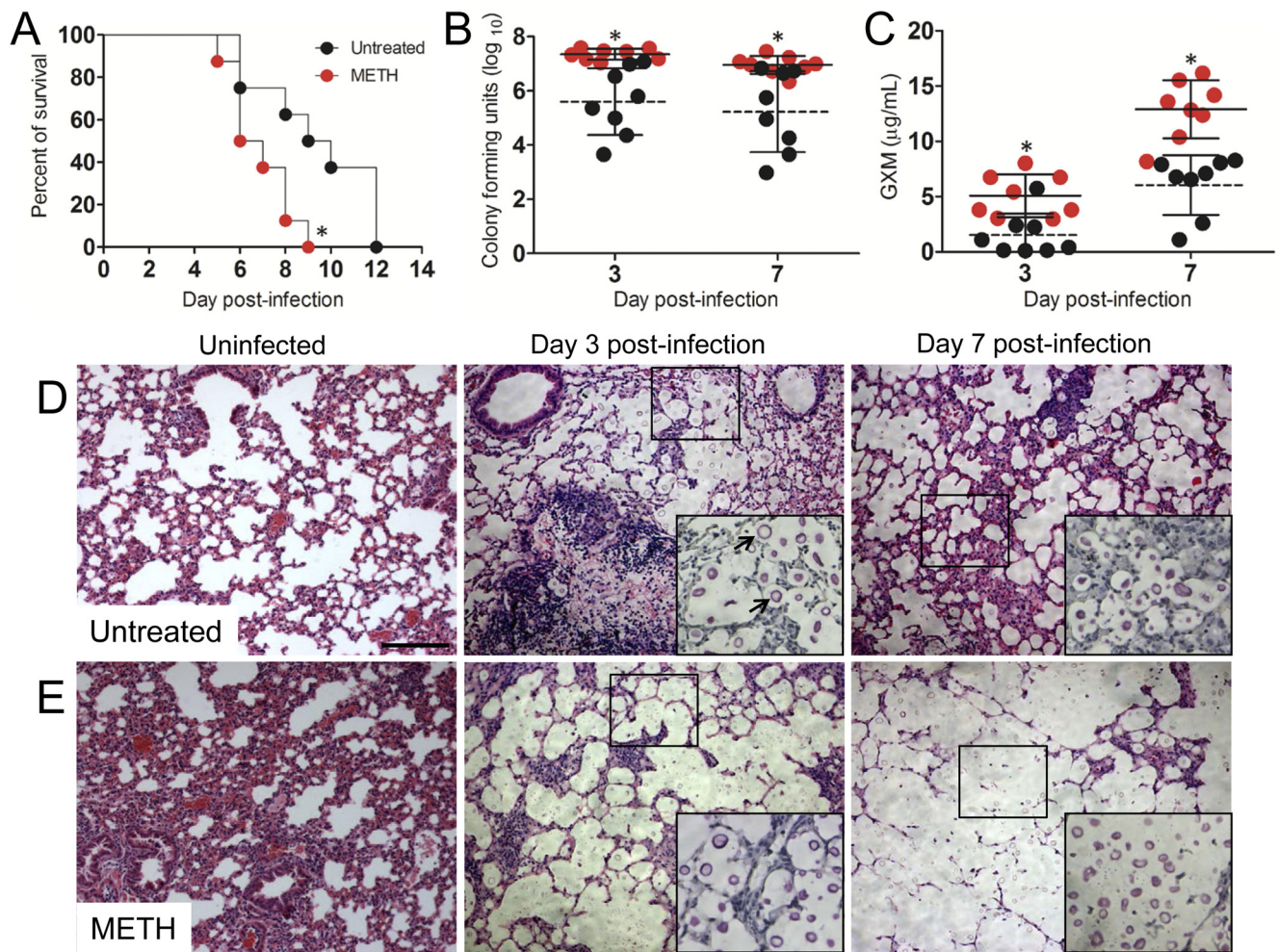
FIG 1 METH exacerbates cryptococcosis. (A) Survival differences of METH- and PBS-injected (untreated, control) C57BL/6 mice after intratracheal (i.t.) infection with 10^7 *C. neoformans* cells (*n* = 5 per group). Asterisks denote *P* value significance (*P* < 0.01) calculated by log rank (Mantel-Cox) analysis. This experiment was performed twice, and similar results were obtained. (B) Lung fungal burden (numbers of CFU) in untreated and METH-treated mice infected with 10^6 *C. neoformans* yeast cells. (C) *C. neoformans* GXM released in lung tissue. (B and C) Each circle represents the value for 1 mouse (*n* = 8 per group). Solid and dashed lines represent average results for METH-treated and untreated groups, respectively. Error bars denote standard deviations. Asterisks denote *P* value significance (*, *P* < 0.05) calculated by Student's *t* test at each time point. These experiments were performed twice with similar results. (D and E) Histological analysis of lungs removed from untreated (D) and METH-injected (E) C57BL/6 mice. Representative H&E-stained sections of the lungs are shown. The large insets are magnifications of the smaller boxes in the H&E-stained sections to better show the cryptococcal cells stained with mucin carmine (indicated with arrows in the middle image of panel D; 3 days postinfection; untreated). Bars, 10 μm.

500 ml) displayed higher capsular mass than controls (359.6 mg/ 500 ml). The glycosyl composition of capsular polysaccharide isolated from METH-treated cultures showed higher quantities of xylose (30 versus 28.1%) and glucose (11.4 versus 3.7%) and lower quantities of glucuronic acid (10.9 versus 11.3%) and mannose (45.8 versus 53.4%) than the glycosyl composition of untreated cultures (Table 1).

METH enhances *C. neoformans* adhesion, capsular polysaccharide release, and biofilm formation. To determine the mechanism by which METH promotes *C. neoformans* adhesion and biofilm formation in the lungs, the spot enzyme-linked immunosorbent assay (ELISA) was utilized. This assay was used to examine local release of capsular polysaccharide by attached cryptococcal cells and the role of this polysaccharide in *C. neoformans* biofilm formation. Light microscopy was used to quantify the number of cells that attached, as measured by spot formation

(Fig. 5A). METH-treated *C. neoformans* cells produced significantly larger numbers of spots than control cells (*P* < 0.05) after a 0.5-h incubation period (Fig. 5B). However, the number of spots observed for control cryptococcal cells increased significantly relative to time, although the number remained significantly less than that for METH-exposed cells at each time interval examined.

In addition, the surface areas of the spots were measured by tracing the circumference of a whole spot left by the organism at the equatorial plane (area = πr^2) (Fig. 5C). This was done to determine the impact of METH on the area involved in the binding of GXM released by attached *C. neoformans* cells. Spots from METH-treated *C. neoformans* cells were significantly larger than those from untreated cells with 50 μM METH after 0.5 h and with 25 μM METH by 1 h of incubation (*P* < 0.001).

C. neoformans strain H99 biofilms treated with METH showed a significant dose-dependent increase in metabolic activity when
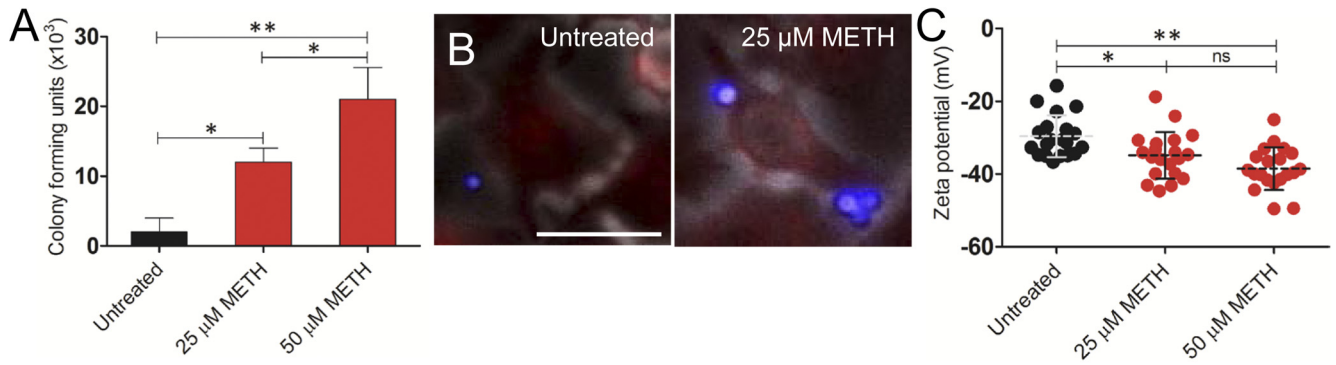
FIG 2 METH enhances fungal adhesion to A549 human epithelial lung cells. (A) Attachment of cryptococcal cells to untreated or METH-treated A549 cells was determined by counting CFU. Bars indicate the averages of the results of three measurements per well ($n = 2$ per condition), and error bars denote standard deviations. Asterisks denote P value significance (*, $P < 0.05$; **, $P < 0.001$) calculated by analysis of variance and adjusted by use of the Bonferroni correction. (B) METH promotes *C. neoformans* adhesion to epithelial cells. After coincubation with 25 μM METH, epithelial cells were washed and incubated with wheat germ agglutinin (WGA) to label sialic acid on cell surfaces (red). Cryptococcal cells were incubated with MAb 18B7-Alexa Fluor-conjugated goat anti-mouse IgG1 stained to label the capsular polysaccharide (blue). Bar, 10 μm. (C) Zeta potential of *C. neoformans* grown with or without METH. Each symbol represents the value for 1 fungal cell ($n = 20$ per group). Dashed lines represent averages of the results. Error bars denote standard deviations. Asterisks denote P value significance (*, $P < 0.05$; **, $P < 0.001$; ns, not significant) calculated by analysis of variance and adjusted by use of the Bonferroni correction. For panels A and C, experiments were performed twice, with similar results.

viability was measured by the 2,3-bis(2-methoxy-4-nitro-5-sulfophenyl)-5-[(phenylamino)carbonyl]-2*H*-tetrazolium-hydroxide (XTT) reduction assay after 5 h of cultivation (Fig. 5D). For example, the metabolic activity of cryptococcal biofilms was increased 2- and 3-fold after treatment with 25 and 50 μM METH, respectively, relative to that of control cells. Confocal microscopic examination was used to correlate the XTT reduction assay results with the visual effects on biofilm metabolism and structure (Fig. 5E). Regions of red fluorescence (FUN-1) represent metabolically active cells, and the green fluorescence (MAb 18B7-
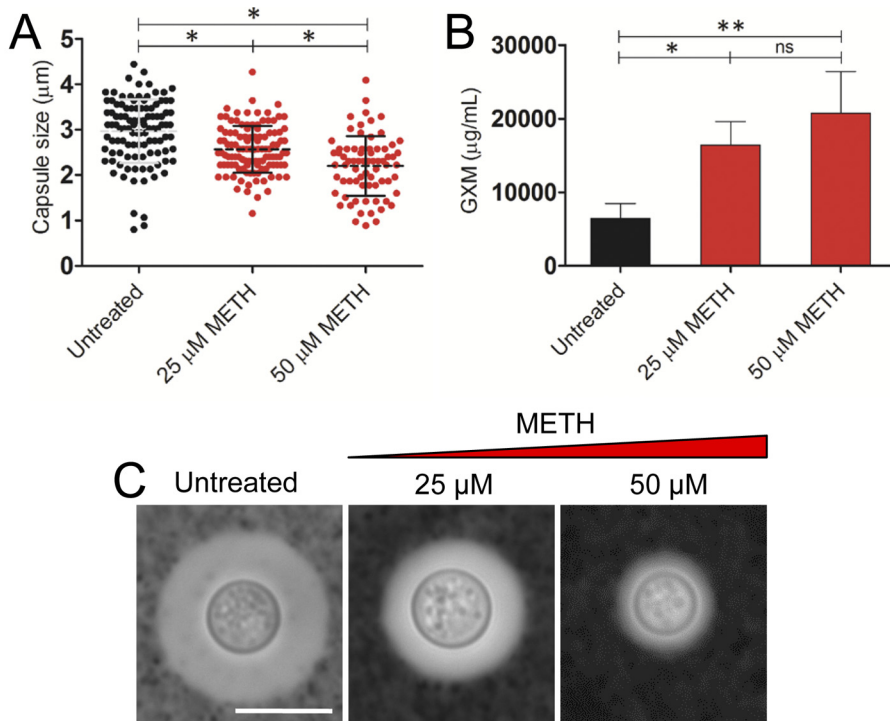
FIG 3 Impact of METH on *C. neoformans* capsular polysaccharide released *in vitro*. (A) Capsule size measurements of *C. neoformans* strain H99 cells were done for cells grown in the absence and presence of 25 and 50 μM/ml METH. The capsule size of 100 cells was measured. (B) GXM concentration in the supernatant of *C. neoformans* cultures coincubated in the absence or presence of METH. (A and B) Averages and standard deviations were determined. Asterisks denote P value significance (*, $P < 0.05$; **, $P < 0.001$) calculated by analysis of variance and adjusted by use of the Bonferroni correction. (C) Representative India ink images displaying the effect of METH on the capsule size of *C. neoformans*. Untreated fungal cells exhibited larger capsules than METH-treated *C. neoformans* cells. The pictures were taken using a ×100-power field. Bar, 2 μm. The experiments were performed twice, and similar results were obtained.
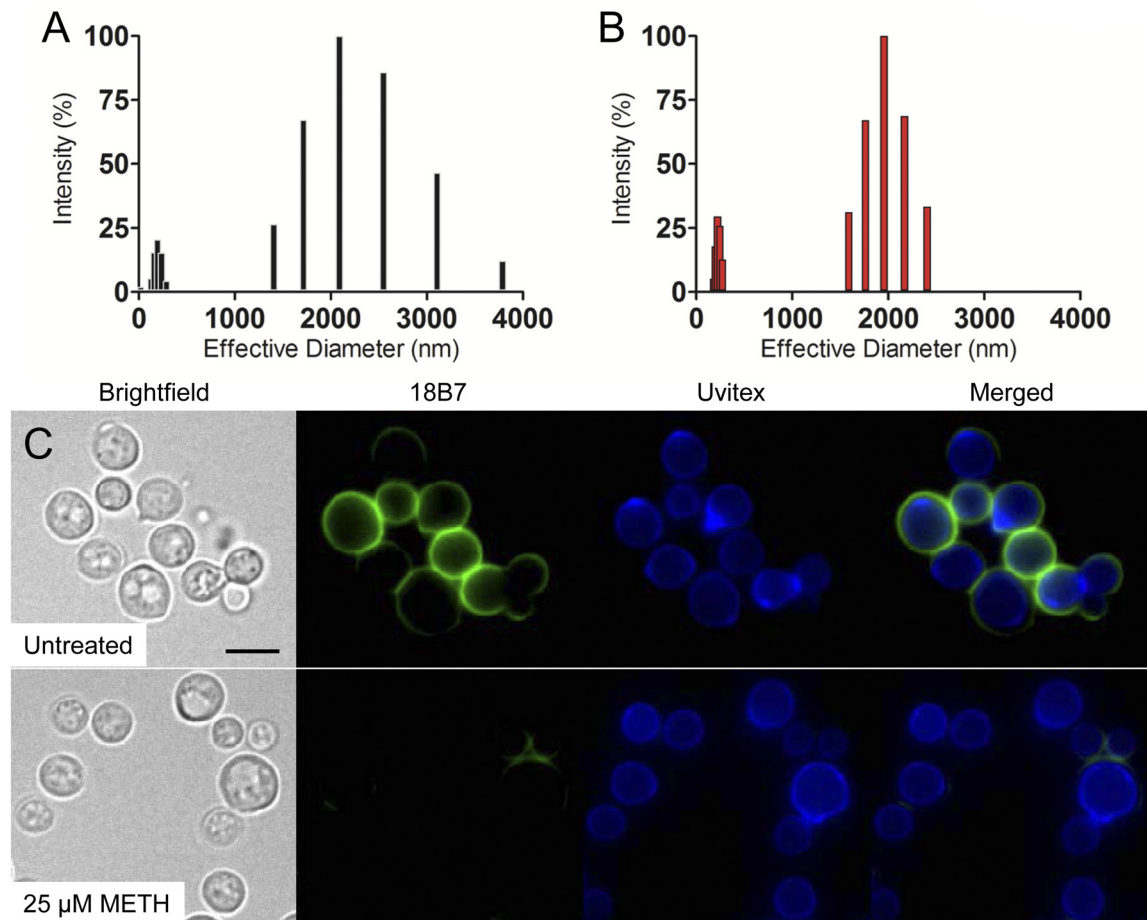
FIG 4 METH alters the size of *C. neoformans* capsular polysaccharide fractions. Capsular polysaccharide obtained from untreated (A) and METH-treated (B) strain H99. The *x* axis represents size distribution by particle diameter; the *y* axis corresponds to the values of percentage intensity-weighted sizes obtained with the nonnegative least-squares (NNLS) algorithm. (C) METH promotes capsular polysaccharide release from cryptococcal cells. After coincubation with 25 μM METH, the cells were washed and incubated with Uvitex and MAb 18B7-FITC-conjugated goat anti-mouse IgG1 stain to label the cell wall (blue) and capsular polysaccharide (green), respectively. Bar, 2 μm.

fluorescein isothiocyanate [FITC]-conjugated goat anti-mouse IgG1) indicates GXM. *C. neoformans* cells incubated with 25 μM METH had regions of high metabolic activity and biofilm formation that were significantly greater than those of cells grown without the drug (Fig. 5E).

METH facilitates *C. neoformans* dissemination from the lungs to the CNS. We investigated the impact of METH on *C. neoformans* dissemination to the brain using a pulmonary model of infection. The fungal counts (Fig. 6A) and quantities of GXM (Fig. 6B) in the brain of METH-treated mice were significantly higher than in control animals 3 days after infection ($P < 0.01$). Immunofluorescence staining showed larger lesions and larger amounts of GXM released in the brains of METH-treated mice than in untreated animals (Fig. 6C). The areas of brain lesions of METH-treated, infected mice reached, on average, 41.87 μm² $\pm$ 3.72 μm², whereas lesions of control mice averaged 19.75 μm² $\pm$ 2.55 μm² ($P < 0.001$) (Fig. 6D).

DISCUSSION

*C. neoformans* enters the host through the respiratory tract and is nearly universally contained in the setting of intact immunity,

TABLE 1 Glycosyl composition analysis of capsular polysaccharide released in culture medium and isolated from untreated or METH-treated *C. neoformans* strain H99

Glycosyl residue	Untreated		25 μM METH	
	Mass (mg)	Mol%[a]	Mass (mg)	Mol%
Ribose (Rib)	3.0	1.0	2.1	0.5
Arabinose (Ara)	ND[b]		ND	
Rhamnose (Rha)	ND		ND	
Fucose (Fuc)	ND		ND	
Xylose (Xyl)	88.3	28.1	134.9	30.0
Glucuronic acid (GlcA)	45.8	11.3	63.6	10.9
Galacturonic acid (GalA)	ND		ND	
Mannose (Man)	201.4	53.4	247.3	45.8
Galactose (Gal)	9.1	2.4	6.6	1.2
Glucose (Glc)	14.1	3.7	61.7	11.4
N-acetylgalactosamine (GalNAc)	ND		ND	
N-acetylglucosamine (GlcNAc)	1.0	0.2	0.6	0.1
N-acetylmannosamine (ManNAc)	ND		ND	
Sum of carbohydrates	359.6		514.5	

[a] Values are expressed as mole percentages of total carbohydrate. The total percentage may not add up to exactly 100% due to rounding.
[b] ND, not detected. Samples for two independent experiments were analyzed, with similar results.
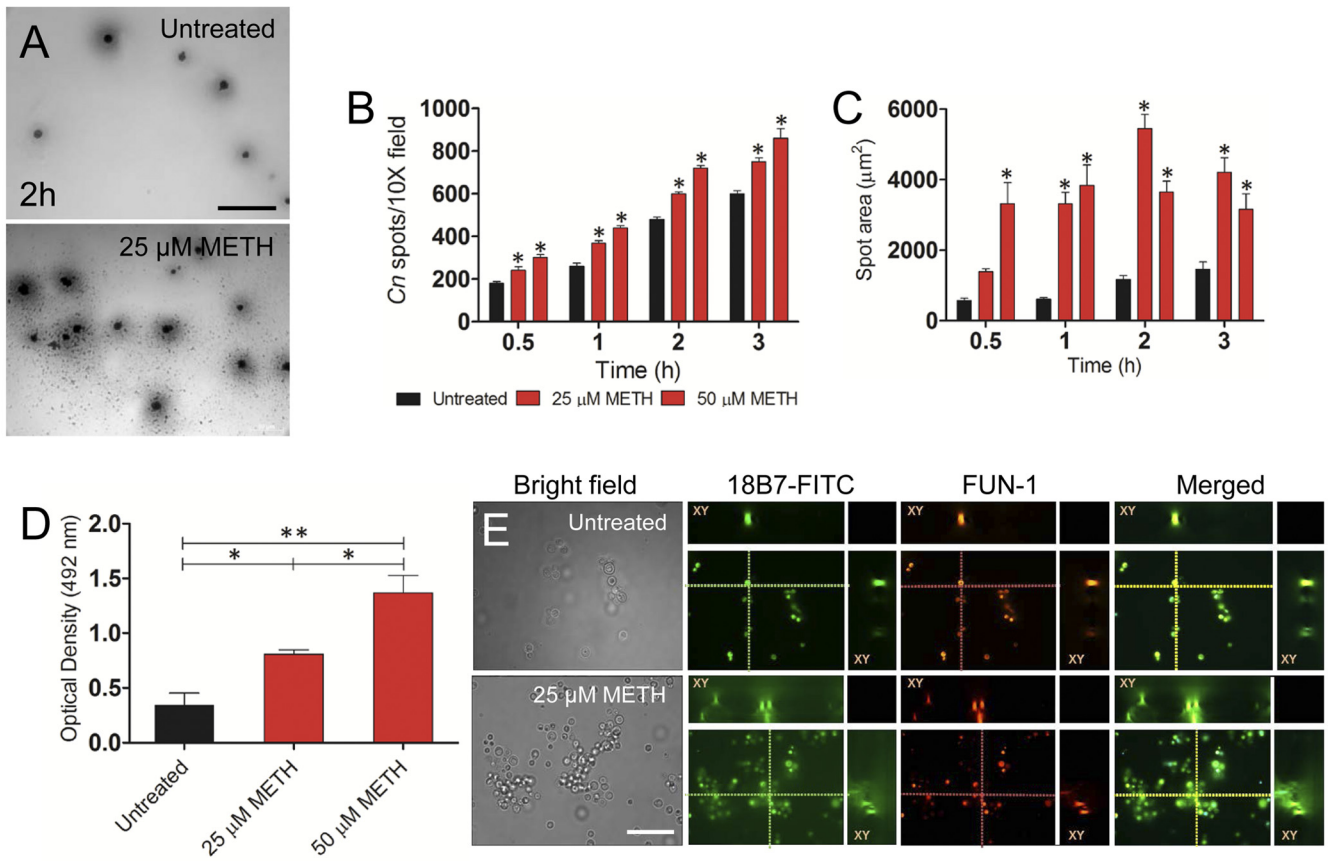
FIG 5 METH stimulates *C. neoformans* GXM release, adhesion, and biofilm formation. (A) Light-microscopic images of spots formed by *C. neoformans* strain H99 cultivated with or without 25 µM METH for 2 h during the spot ELISA. The pictures were taken by using a ×20-power field. Bars, 10 µm. The results are representative of two experiments. (B) Spot number in microtiter wells as a function of time after treatment with 25 and 50 µM METH. Bars are the average numbers of spots in five ×20-power fields, and error bars denote standard deviations. *, $P < 0.05$ in a comparison of the untreated and METH-treated groups. *Cn*, *C. neoformans*. (C) The release of *C. neoformans* GXM was visualized by the spot ELISA with or without exposure of the yeast cells for 0.5, 1, 2, and 3 h to two concentrations (25 and 50 µM) of METH. Bars are the averages of the areas of 40 spots per ×20-power field, with the area being calculated with the equation πr^2. Five power fields were observed for each time interval. Error bars denote standard deviations. *, $P < 0.001$ in a comparison of untreated and METH-treated groups. (D) Metabolic activities of untreated and METH-treated *C. neoformans* biofilms measured by the XTT reduction assay. Yeast cells were incubated with or without 25 and 50 µM METH for 48 h. Bars are the averages of five XTT measurements, and error bars denote standard deviations. *, $P < 0.05$; **, $P < 0.001$. This experiment was performed twice, and similar results were obtained. (E) Confocal microscopy of *C. neoformans* biofilms not treated or treated with METH. Orthogonal images of mature *C. neoformans* biofilms showed metabolically active (red; FUN-1-stained) cells embedded in the polysaccharide extracellular material (green; stained with MAb 18B7-FITC-conjugated goat anti-mouse IgG1). Images were obtained after 48 h of exposure of the fungal cells to 25 µM METH, and the images were compared with those of biofilms incubated in the presence of PBS (untreated). The pictures were taken at a magnification of ×63. Bars, 20 µm. The results are representative of two distinct experiments.

whereas the fungus can cause a pulmonary disease that may progress and disseminate to the CNS in immunocompromised hosts, especially in the setting of AIDS. A recent report has revealed a greater risk for tuberculosis (TB) among METH users than non-users (23). Similarly, a study of HIV-infected patients in Thailand reported that 40% of those also infected with TB had a history of METH use (24). In addition, we have demonstrated that METH enhances disease caused by the pathogenic intracellular fungus *Histoplasma capsulatum* (25). In the present study, we further investigated whether METH enhances host susceptibility to a pulmonary infection such as cryptococcosis. Our results showed that METH significantly enhances the mortality of *C. neoformans*-infected mice, fungal burden, and the amount of *C. neoformans* capsular polysaccharide released *in vivo*. These findings lead us to hypothesize that METH stimulates fungal biofilm formation in the lungs of treated animals, which may serve as a reservoir for *C.*

neoformans evasion of immunity, enhancing fungal survival and facilitating subsequent dissemination to the CNS.

Recently, Volkow et al. demonstrated that the lungs have the highest METH uptake and most rapid clearance compared to other organs after intravenous injection (8). METH is associated with elevated free radical formation and significant lung injury (26). Although we observed a reduction in alveolar space in the lungs of METH-treated mice prior to infection, we recently showed that METH administration does not alter the numbers of neutrophils or macrophages in lung tissues (7), which may reflect a combination of the sporadic presence of the drug and the responsive migration of these cells in this tissue. Additionally, we have previously shown that METH alters innate immune cell effector functions such as phagocytosis and antigen processing (27, 28). Our results show that accumulation of METH in the lungs may also contribute by rendering pulmonary tissue more vulner-
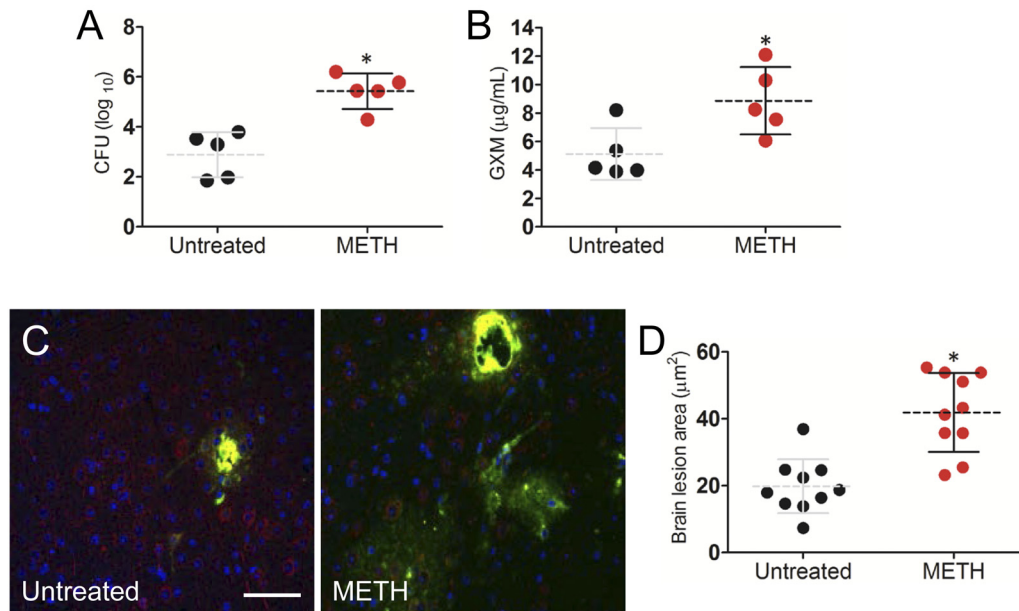
FIG 6 METH significantly induces *C. neoformans* capsular polysaccharide release in the CNS 3 days after pulmonary infection. (A) The brain fungal burdens in METH-treated mice infected intratracheally with 10^6 *C. neoformans* cells were significantly greater than those in untreated mice ($n = 5$ per group). (B) Capsular polysaccharide concentrations in the supernatants of *C. neoformans*-infected brain homogenates of untreated or METH-treated mice ($n = 5$ per group). (A and B) Dashed lines represent the mean values for the METH-treated and untreated groups; error bars denote standard deviations. Each circle represents the value for 1 mouse. *P* values (*, $P < 0.05$) were calculated by Student's *t* test. (C) Immunofluorescence staining of brain lesions (cryptococcomas) caused by *C. neoformans* in untreated or METH-treated animals. Capsular-polysaccharide-specific MAb 18B7 (yellow) was used to label fungal cells. MAP-2 (red) and DAPI (blue) staining were used to label the cell bodies and nuclei of neurons, respectively. Bar, 5 μm. (D) Area analyses of brain lesions caused by *C. neoformans* strain H99 cells were performed in tissue sections of untreated or METH-treated mice ($n = 3$ per group). The areas of 10 brain lesions per condition were measured using ImageJ software. Each circle represents a single lesion. Dashed lines and error bars denote averages of 10 measurements and standard deviations, respectively. Asterisks denote *P* value significance (*, $P < 0.001$) calculated by the *t* test. (A to D) The experiments were performed twice, with similar results.

able to infections due to defects in macrophages and neutrophils. In this regard, our histological analysis of the lungs showed that, in contrast to controls, METH-treated mice displayed low numbers of inflammatory cells in the pulmonary tissue early during infection and large numbers of cryptococci surrounded by vast amounts of polysaccharide in a biofilm-like arrangement 7 days postinfection. Notably, we documented that METH-treated animals had more-accelerated breathing than controls, suggesting respiratory distress due to the infection.

To determine the mechanism by which METH stimulates *C. neoformans* adhesion to pulmonary tissue, we incubated A549 cells with the drug and evaluated fungal adhesion. We observed that METH enhanced yeast adhesion to these epithelial cells, suggesting that the drug causes cellular alterations in A549 cells. A decrease in the negative surface charge has been shown to increase significantly the adhesion of several microbes to host tissues (29). This fact may play an important role in the lungs of METH-treated mice, where the increased adherence of *C. neoformans* in human airways might stimulate biofilm formation, leading to chronic lung infection. In patients with cystic fibrosis, adhesion of bacterial pathogens increases due to a reduction in the negativity of the epithelial cell surface charge (30). METH might modify the negative charge by membrane phospholipids, surface carbohydrates, and ionized groups of membrane proteins. Although this is beyond the scope of this report, it might be a logical and interesting extension of this work to evaluate in our future investigations.

METH stimulates *C. neoformans* biofilm formation *in vivo*. The polysaccharide capsule of *C. neoformans* is responsible for the high negative charge of the cells (21). Our zeta potential analysis demonstrates that METH imparts a high negative charge to the cryptococcal surface, which may translate into enhanced interaction with pulmonary tissue colonization or adhesion and yeast cell-cell interactions during biofilm formation (31). For instance, a mutant of the thermophile *Anoxybacillus flavithermus* showing a reduced negative charge and hydrophobic cell membrane displayed an impaired ability to adhere to a solid surface (32). Similarly, we have previously shown that cationic chitosan reduces biofilm formation in *C. neoformans* (31) and *Candida albicans* (33).

The release of the cryptococcal polysaccharide capsule is important for adhesion of the yeast and biofilm development in *C. neoformans* (13). An spot ELISA provided an alternate method to confirm the results obtained *in vivo* and *in vitro* in establishing the mechanism by which METH promotes *C. neoformans* colonization and biofilm formation. The numbers and areas of spots on microtiter plates were determined as a function of time using light microscopy. Biofilm formation by *C. neoformans* did correlate with the number of yeast cells bound to the plastic support surface and GXM released. For instance, *C. neoformans* biofilms grown in the presence of METH attached in larger quantities to the plastic surface of the microtiter plate and produced larger spots than control biofilms. This result implies that METH stimulates fungal local release of capsular polysaccharide by attached cells and biofilm formation in the respiratory tract. In fact, the combination of extensive *C. neoformans* capsular polysaccharide release impairs innate immune cell migration (11), and the immunosuppressive

effect of the drug may have detrimental effects on METH users with AIDS.

We assessed the effect of METH on *C. neoformans* capsular polysaccharide, which is essential for pathogenesis (34). Interestingly, fungal cells treated with 25 μM METH showed a punctate or limited GXM-binding pattern with MAb 18B7, as opposed to the annular pattern exhibited by untreated cells. Studies by Feldmesser et al. (35) showed that differences in levels of GXM binding by MAbs are related to the efficacies of those antibodies in protecting *C. neoformans*-infected animals. For instance, an annular GXM binding pattern is indicative of protection, whereas punctate binding is indicative of the opposite. Similarly, there were differences in the fluorescence intensities displayed. Untreated cells showed a larger and very well delineated capsule compared to METH-treated cells. In this regard, structural studies using light scattering revealed that capsular polysaccharide molecules on METH-treated fungal cells were shorter than those on their untreated counterparts. Moreover, we observed more-homogeneous fibers of polysaccharide in fungal cells exposed to METH than in control cells. This observation was further supported by a capture ELISA that demonstrated that METH-treated cells released the capsular polysaccharide in significantly higher quantities than untreated cells. Furthermore, we performed structural studies on the exopolysaccharides of untreated and METH-treated *C. neoformans* cells. Sugar composition analysis of METH-treated yeast cells was remarkable for the predominance of xylose and glucose, whereas untreated capsular polysaccharide consisted of high levels of glucuronic acid, mannose, and galactose. Our results suggest that a drug of abuse may cause alterations in the production of a virulence factor by a pathogen and the adaptive capacity of microorganisms to external stimuli, which can be advantageous to the microbe during pathogenesis.

We investigated the impact of METH on *C. neoformans* dissemination from the lungs to the CNS using an intratracheal model of METH abuse and infection. *C. neoformans* is a neurotropic fungus; therefore, our findings demonstrated high numbers of CFU, levels of GXM, and brain lesions in METH-treated mice. METH is present in the brain within 9 min after exposure, and the drug is maintained for protracted periods thereafter (36). Recently, we showed that METH modifies tight junction and adhesion molecules, increasing the permeability of the BBB and facilitating CNS invasion by *C. neoformans* using an intravenous model of infection (20). It is also well documented that METH-induced oxidative stress and hyperthermia are primary factors underlying the damage of neural cells (37, 38) and associated leakage of the BBB. In fact, METH contributes to host neurotoxicity by causing morphological abnormalities to the components of the BBB, therefore, facilitating microbial CNS invasion (37). Similarly, from the side of the pathogen, we have previously hypothesized that GXM release may also be influenced by Ca^{2+} sequestration from endothelial cells on the BBB, leading to GXM-mediated BBB disruption and enhanced fungal invasion (20). Molecular and cellular abnormalities of the cells that compose the BBB (39) may also arise from the interaction and accumulation of fungal cells. In this regard, we have documented increased fungemia in the bloodstream of METH-infected mice. Likewise, *C. neoformans* can use a "Trojan horse" mechanism (19) to cross the brain vasculature by transmigrating within macrophages, which is also consistent with our model.

In conclusion, METH promotes *C. neoformans* colonization of the lungs upon infection and subsequent biofilm formation. Our findings suggest that *C. neoformans* biofilms may act as a fungal reservoir, shielding single cells from phagocytic cells, which can later disseminate, especially to the CNS. Moreover, the drug causes profound defects in the integrity of the BBB *in vivo*, increasing permeability and facilitating the transmigration of *C. neoformans* to the CNS. METH-induced alterations to the molecules responsible for maintaining the integrity of the BBB provide an explanation for the susceptibility of a METH abuser to brain infection by HIV and other pathogens. Broadly, METH has diverse and pronounced detrimental effects on host immunity that can also enhance pathogen persistence and proliferation.

MATERIALS AND METHODS

C. neoformans. *C. neoformans* strain H99 (serotype A) was inoculated in Sabouraud dextrose broth (Difco, MI) and incubated at 30°C for 24 h in a rotary shaker set at 150 rpm (Cole-Parmer, IL).

Methamphetamine administration. High-dose-METH users initially take small amounts of the drug intermittently before progressively increasing the dose (40). To simulate this pattern, increasing doses (2.5, 5, and 10 mg/kg of body weight/day at weeks 1, 2, and 3, respectively) of METH (Sigma, MO) were intraperitoneally (i.p.) administered daily to female C57BL/6 mice (age, 6 to 8 weeks; NCI) over 21 days. Phosphate-buffered saline (PBS)-treated animals were used as controls. Animal care for this study was approved by the Animal Welfare and Research Ethics Committee at the Albert Einstein College of Medicine (protocol number 20110402).

In vivo **pulmonary model and *C. neoformans* infection.** At day 21, METH- and PBS-treated C57BL/6 mice were anesthetized with 100 mg/kg ketamine (Ketaset; Fort Dodge, IA) and 10 mg/kg xylazine (AnaSed; Shenandoah, IA). Thereafter, a 100-μl suspension containing either 10^6 or 10^7 *C. neoformans* H99 cells in PBS was inoculated intratracheally (i.t.). For infection with 10^6 cryptococci, animals were euthanized at days 3 and 7 and lung tissues were excised for processing for histology, determination of CFU numbers, and quantification of GXM.

CFU determinations. At day 3 and 7 postchallenge with 10^6 fungal cells, lung tissues were excised from euthanized mice and one lobe of lung was homogenized in sterile PBS. Suspensions were plated on Sabouraud dextrose agar (Difco) and incubated at 30°C for 48 h. Quantification of viable yeast cells was determined by CFU counting.

Histological examinations. At day 3 and 7 postinfection, lung tissues were excised from euthanized mice; the tissues were fixed in 10% formalin for 24 h, processed, and embedded in paraffin. Four-micrometer vertical sections were cut and then fixed to glass slides and subjected either to hematoxylin and eosin (H&E) stain or to mucin carmine (MC) stain, in order to examine tissue and fungal morphology, respectively. Microscopic examinations of tissues were performed by light microscopy.

Human epithelial cells The human type II alveolar-epithelial-cell-like cell line A549 (ATCC, VA) was used in this study. These cells are derived from lung carcinomatous tissue and are widely used in cell models to study infection by respiratory pathogens (41). The cell cultures were maintained as previously described (27). A549 cells were then incubated in the absence or the presence of 25 μM METH for 2 h at 37°C in 5% CO_2. *C. neoformans* adhesion was assessed by CFU determination as previously described (27).

***C. neoformans* capsular polysaccharide determinations.** *C. neoformans* capsular GXM released in pulmonary tissue and culture was measured by capture ELISA as described previously (22).

Capsule measurement. An aliquot of 10 μl of untreated or METH-treated yeast cells was mixed with India ink and visualized with light microscopy. The capsule size of 100 cells was measured in these images using ImageJ 1.39u software (NIH). Capsule size was defined as the difference between the diameter of the total cell (capsule included) and the cell body diameter, defined by the cell wall.

Isolation of exopolysaccharide from culture supernatants by filtration. Polysaccharide was isolated by filtration and ultrafiltration as described previously (42).

Release of capsular components by DMSO. Capsular polysaccharide was isolated from yeast cells with dimethyl sulfoxide (DMSO) as previously described (43). The final polysaccharide solution was lyophilized and the dry polysaccharide mass determined.

Polysaccharide particle sizes. The effective diameter and the polydispersity of polysaccharide preparations were measured by quasi-elastic light scattering in a 90Plus/BI-MAS multiangle, particle-sizing analyzer (Brookhaven Instruments Corp., NY) as previously described (31).

Zeta potential measurement. The zeta potential (ζ), particle mobility, and shift frequency of polysaccharide samples were calculated in a Zeta potential analyzer (ZetaPlus; Brookhaven Instruments) as previously described (31).

Glycosyl composition analysis of matrix material. Glycosyl composition analysis was performed by combined gas chromatography-mass spectrometry of the per-*O*-trimethylsilyl derivatives of the monosaccharide methyl glycosides produced from the sample by acidic methanolysis as previously described (44).

Spot ELISA. *C. neoformans* H99 cells were allowed to adhere to the bottoms of the wells over a series of time intervals (0.5, 1, 2, and 3 h) in the absence and the presence of 25 or 50 μM METH. Following the adhesion stage, the wells containing *C. neoformans* biofilms were washed and processed as described previously (13, 15, 31).

Biofilm formation. *C. neoformans* cells were incubated in the absence or presence of 25 μM METH at 37°C. Biofilm formation occurred by 48 h and was quantified using the 2,3-bis(2-methoxy-4-nitro-5-sulfophenyl)-5-[(phenylamino)carbonyl]-2*H*-tetrazolium-hydroxide (XTT; Sigma) reduction assay as previously described (13–15, 31, 33, 44).

Imaging. (i) Light microscopy. Microscopic examinations of individual fungal cells and tissues were performed by light microscopy with an Axiovert 40-CFL inverted microscope (Carl Zeiss, NY) and photographed with an AxioCam MrC digital camera using Zen 2011 digital imaging software (Carl Zeiss).

(ii) Fluorescence microscopy. For immunofluorescence studies, slides were coated with poly-L-lysine (0.1 mg/ml; Sigma), and 10^6 yeast cells were allowed to air dry on slides so that organisms adhered. Chitin in the cell wall was visualized using Uvitex 2B. The IgG1 GXM-specific monoclonal antibody (MAb) 18B7 was added at 2 μg/ml in buffer (PBS with 1% bovine serum albumin [BSA]). Fluorescein isothiocyanate (FITC)-labeled goat anti-mouse (GAM)-IgG1 (Southern Biotechnology, AL) was added at 2 μg/ml after application of unconjugated MAb. All incubations were done at 37°C for 30 min, and slides were washed three times with PBS between applications of reagents. Slides were washed again with PBS, 30 μl of mounting medium (0.1 M *n*-propyl gallate–50% glycerol in PBS) was added, and coverslips were placed. The slides were then viewed, and fluorescent images were recorded.

(iii) Epifluorescence microscopy. *C. neoformans* biofilms were incubated for 45 min in 75 μl of PBS containing the fluorescent stain FUN-1 (10 μM). Then, wells were blocked with PBS (1% BSA). MAb 18B7 (44, 45) (2 μg/ml) was added, and the plate was incubated. FITC-conjugated GAM IgG1 (Fisher Scientific) at a 1-μg/ml concentration in PBS (1% BSA) was applied. Between steps, the wells were washed with 0.05% Tween 20 in TBS. All incubations were done at 37°C for 1 h. FUN-1 (excitation wavelength, 470 nm; emission, 590 nm) is converted to orange-red cylindrical intravacuolar structures by metabolically active cells, while MAb 18B7, when bound by FITC-conjugated GAM IgG1 (excitation wavelength, 488 nm; emission, 530 nm), labels GXM and fluoresces green. Microscopic examinations of biofilms formed in microtiter plates were performed with epifluorescence microscopy using an Axiovert 200 M inverted microscope (Carl Zeiss) as previously described (13–15, 31, 33, 44).

(iv) Confocal microscopy. *C. neoformans* cells and capsular polysaccharide released in tissue were stained using MAb 18B7. Slides were blocked, and 18B7 (2 μg/ml) was added for 1 h at 37°C. After the slides were washed, FITC-conjugated GAM antibody (1:250; 1% BSA) was applied for 1 h at room temperature. Neurons in tissue sections were stained with DAPI (4′,6-diamidino-2-phenylindole) and MAP-2 as described previously (20). Microscopic examinations of brain sections were performed with a fully motorized Axio Observer Z1 confocal microscope (Carl Zeiss). Confocal images of blue, green, and red fluorescence were conceived simultaneously using a multichannel mode. Z-stack images and measurements were corrected utilizing Zen software in deconvolution mode.

Statistical analysis. Data were analyzed using Prism (GraphPad, CA). P values of <0.05 were considered significant.

REFERENCES

1. **Gonzales R, Mooney L, Rawson RA.** 2010. The methamphetamine problem in the United States. Annu. Rev. Public Health **31:**385–398.
2. **Cherner M, Letendre S, Heaton RK, Durelle J, Marquie-Beck J, Gragg B, Grant I, HIV Neurobehavioral Research Center Group.** 2005. Hepatitis C augments cognitive deficits associated with HIV infection and methamphetamine. Neurology **64:**1343–1347.
3. **Carey CL, Woods SP, Rippeth JD, Gonzalez R, Heaton RK, Grant I.** 2006. Additive deleterious effects of methamphetamine dependence and immunosuppression on neuropsychological functioning in HIV infection. AIDS Behav. **10:**185–190.
4. **Urbina JA, Concepcion JL, Caldera A, Payares G, Sanoja C, Otomo T, Hiyoshi H.** 2004. *In vitro* and *in vivo* activities of E5700 and ER-119884, two novel orally active squalene synthase inhibitors, against *Trypanosoma cruzi*. Antimicrob. Agents Chemother. **48:**2379–2387.
5. **Ellis RJ, Childers ME, Cherner M, Lazzaretto D, Letendre S, Grant I, HIV Neurobehavioral Research Center Group.** 2003. Increased human immunodeficiency virus loads in active methamphetamine users are explained by reduced effectiveness of antiretroviral therapy. J. Infect. Dis. **188:**1820–1826.
6. **Gonzales R, Marinelli-Casey P, Shoptaw S, Ang A, Rawson RA.** 2006. Hepatitis C virus infection among methamphetamine-dependent individuals in outpatient treatment. J. Subst. Abuse Treat. **31:**195–202.
7. **Peerzada H, Gandhi JA, Guimaraes AJ, Nosanchuk JD, Martinez LR.** 2013. Methamphetamine administration modifies leukocyte proliferation and cytokine production in murine tissues. Immunobiology **218:** 1063–1068.
8. **Volkow ND, Fowler JS, Wang GJ, Shumay E, Telang F, Thanos PK, Alexoff D.** 2010. Distribution and pharmacokinetics of methamphetamine in the human body: clinical implications. PLoS One **5:**e15269. doi: 10.1371/journal.pone.0015269.
9. **Park BJ, Wannemuehler KA, Marston BJ, Govender N, Pappas PG, Chiller TM.** 2009. Estimation of the current global burden of cryptococcal meningitis among persons living with HIV/AIDS. AIDS **23:**525–530.
10. **Zaragoza O, Nielsen K.** 12 April 2013. Titan cells in Cryptococcus neoformans: cells with a giant impact. Curr. Opin. Microbiol. doi: 10.1016/j.mib.2013.03.006.
11. **Casadevall A, Perfect J.** 1998. Cryptococcus neoformans. ASM Press, Washington, DC.
12. **Vecchiarelli A.** 2000. Immunoregulation by capsular components of Cryptococcus neoformans. Med. Mycol. **38:**407–417.
13. **Martinez LR, Casadevall A.** 2005. Specific antibody can prevent fungal

biofilm formation and this effect correlates with protective efficacy. Infect. Immun. **73**:6350–6362.

14. **Martinez LR, Casadevall A.** 2006. Cryptococcus neoformans cells in biofilms are less susceptible than planktonic cells to antimicrobial molecules produced by the innate immune system. Infect. Immun. **74**: 6118–6123.

15. **Martinez LR, Casadevall A.** 2006. Susceptibility of Cryptococcus neoformans biofilms to antifungal agents *in vitro*. Antimicrob. Agents Chemother. **50**:1021–1033.

16. **Dromer F, Mathoulin-Pélissier S, Launay O, Lortholary O, French Cryptococcosis Study Group.** 2007. Determinants of disease presentation and outcome during cryptococcosis: the CryptoA/D study. PLoS Med. **4**:e21. doi:10.1371/journal.pmed.0040021.

17. **Lortholary O, Improvisi L, Rayhane N, Gray F, Fitting C, Cavaillon JM, Dromer F.** 1999. Cytokine profiles of AIDS patients are similar to those of mice with disseminated *Cryptococcus neoformans* infection. Infect. Immun. **67**:6314–6320.

18. **Chang YC, Stins MF, McCaffery MJ, Miller GF, Pare DR, Dam T, Paul-Satyaseela M, Kim KS, Kwon-Chung KJ, Paul-Satyasee M.** 2004. Cryptococcal yeast cells invade the central nervous system via transcellular penetration of the blood-brain barrier. Infect. Immun. **72**:4985–4995.

19. **Charlier C, Nielsen K, Daou S, Brigitte M, Chretien F, Dromer F.** 2009. Evidence of a role for monocytes in dissemination and brain invasion by *Cryptococcus neoformans*. Infect. Immun. **77**:120–127.

20. **Eugenin EA, Greco JM, Frases S, Nosanchuk JD, Martinez LR.** 2013. Methamphetamine alters blood brain barrier protein expression in mice, facilitating central nervous system infection by neurotropic Cryptococcus neoformans. J. Infect. Dis. doi:10.1093/infdis/jit117.

21. **Nosanchuk JD, Casadevall A.** 1997. Cellular charge of *Cryptococcus neoformans*: contributions from the capsular polysaccharide, melanin, and monoclonal antibody binding. Infect. Immun. **65**:1836–1841.

22. **Martinez LR, Moussai D, Casadevall A.** 2004. Antibody to *Cryptococcus neoformans* glucuronoxylomannan inhibits the release of capsular antigen. Infect. Immun. **72**:3674–3679.

23. **Pevzner ES, Robison S, Donovan J, Allis D, Spitters C, Friedman R, Ijaz K, Oeltmann JE.** 2010. Tuberculosis transmission and use of methamphetamines in Snohomish County, WA, 1991–2006. Am. J. Public Health **100**:2481–2486.

24. **Mankatittham W, Likanonsakul S, Thawornwan U, Kongsanan P, Kittikraisak W, Burapat C, Akksilp S, Sattayawuthipong W, Srinak C, Nateniyom S, Tasaneeyapan T, Varma JK.** 2009. Characteristics of HIV-infected tuberculosis patients in Thailand. Southeast Asian J. Trop. Med. Public Health **40**:93–103.

25. **Martinez LR, Mihu MR, Gácser A, Santambrogio L, Nosanchuk JD.** 2009. Methamphetamine enhances histoplasmosis by immunosuppression of the host. J. Infect. Dis. **200**:131–141.

26. **Wells SM, Buford MC, Braseth SN, Hutchison JD, Holian A.** 2008. Acute inhalation exposure to vaporized methamphetamine causes lung injury in mice. Inhal. Toxicol. **20**:829–838.

27. **Barbosa FM, Fonseca FL, Holandino C, Alviano CS, Nimrichter L, Rodrigues ML.** 2006. Glucuronoxylomannan-mediated interaction of Cryptococcus neoformans with human alveolar cells results in fungal internalization and host cell damage. Microbes Infect. **8**:493–502.

28. **Tallóczy Z, Martinez J, Joset D, Ray Y, Gácser A, Toussi S, Mizushima N, Nosanchuk JD, Goldstein H, Loike J, Sulzer D, Santambrogio L, Santambrogio L.** 2008. Methamphetamine inhibits antigen processing, presentation, and phagocytosis. PLoS Pathog. **4**:e28. doi:10.1371/journal.ppat.0040028.

29. **Nagao PE, Costa e Silva-Filho F, Benchetrit LC, Barrucand L.** 1995. Cell surface hydrophobicity and the net electric surface charge of group B

streptococci: the role played in the micro-organism-host cell interaction. Microbios **82**:207–216.

30. **Thethi K, Duszyk M.** 1997. Decreased cell surface charge in cystic fibrosis epithelia. Cell Biochem. Funct. **15**:35–38.

31. **Martinez LR, Mihu MR, Han G, Frases S, Cordero RJ, Casadevall A, Friedman AJ, Friedman JM, Nosanchuk JD.** 2010. The use of chitosan to damage Cryptococcus neoformans biofilms. Biomaterials **31**:669–679.

32. **Palmer JS, Flint SH, Schmid J, Brooks JD.** 2010. The role of surface charge and hydrophobicity in the attachment of Anoxybacillus flavithermus isolated from milk powder. J. Ind. Microbiol. Biotechnol. **37**: 1111–1119.

33. **Martinez LR, Mihu MR, Tar M, Cordero RJ, Han G, Friedman AJ, Friedman JM, Nosanchuk JD.** 2010. Demonstration of antibiofilm and antifungal efficacy of chitosan against candidal biofilms, using an *in vivo* central venous catheter model. J. Infect. Dis. **201**:1436–1440.

34. **Fromtling RA, Shadomy HJ, Jacobson ES.** 1982. Decreased virulence in stable, acapsular mutants of Cryptococcus neoformans. Mycopathologia **79**:23–29.

35. **Feldmesser M, Rivera J, Kress Y, Kozel TR, Casadevall A.** 2000. Antibody interactions with the capsule of *Cryptococcus neoformans*. Infect. Immun. **68**:3642–3650.

36. **Fowler JS, Volkow ND, Logan J, Alexoff D, Telang F, Wang GJ, Wong C, Ma Y, Kriplani A, Pradhan K, Schlyer D, Jayne M, Hubbard B, Carter P, Warner D, King P, Shea C, Xu Y, Muench L, Apelskog K.** 2008. Fast uptake and long-lasting binding of methamphetamine in the human brain: comparison with cocaine. Neuroimage **43**:756–763.

37. **Kiyatkin EA, Sharma HS.** 2009. Acute methamphetamine intoxication: brain hyperthermia, blood-brain barrier, brain edema, and morphological cell abnormalities. Int. Rev. Neurobiol. **88**:65–100.

38. **Ramirez SH, Potula R, Fan S, Eidem T, Papugani A, Reichenbach N, Dykstra H, Weksler BB, Romero IA, Couraud PO, Persidsky Y.** 2009. Methamphetamine disrupts blood-brain barrier function by induction of oxidative stress in brain endothelial cells. J. Cereb. Blood Flow Metab. **29**:1933–1945.

39. **Kaczmarek A, Vandenabeele P, Krysko DV.** 2013. Necroptosis: the release of damage-associated molecular patterns and its physiological relevance. Immunity **38**:209–223.

40. **Simon SL, Richardson K, Dacey J, Glynn S, Domier CP, Rawson RA, Ling W.** 2002. A comparison of patterns of methamphetamine and cocaine use. J. Addict. Dis. **21**:35–44.

41. **Hahn HP.** 1997. The type-4 pilus is the major virulence-associated adhesin of Pseudomonas aeruginosa—a review. Gene **192**:99–108.

42. **Nimrichter L, Frases S, Cinelli LP, Viana NB, Nakouzi A, Travassos LR, Casadevall A, Rodrigues ML.** 2007. Self-aggregation of *Cryptococcus neoformans* capsular glucuronoxylomannan is dependent on divalent cations. Eukaryot. Cell **6**:1400–1410.

43. **Bryan RA, Zaragoza O, Zhang T, Ortiz G, Casadevall A, Dadachova E.** 2005. Radiological studies reveal radial differences in the architecture of the polysaccharide capsule of *Cryptococcus neoformans*. Eukaryot. Cell **4**:465–475.

44. **Martinez LR, Casadevall A.** 2007. Cryptococcus neoformans biofilm formation depends on surface support and carbon source and reduces fungal cell susceptibility to heat, cold, and UV light. Appl. Environ. Microbiol. **73**:4592–4601.

45. **Casadevall A, Cleare W, Feldmesser M, Glatman-Freedman A, Goldman DL, Kozel TR, Lendvai N, Mukherjee J, Pirofski LA, Rivera J, Rosas AL, Scharff MD, Valadon P, Westin K, Zhong Z.** 1998. Characterization of a murine monoclonal antibody to *Cryptococcus neoformans* polysaccharide that is a candidate for human therapeutic studies. Antimicrob. Agents Chemother. **42**:1437–1446.